



島根大学学術情報リポジトリ

S W A N

Shimane University Web Archives of kNnowledge

Title

Effects and dynamic characteristics of the core-suspended isolation system assessed by long-term structural health monitoring

Author(s)

Yutaka Nakamura, Keiichi Okada

Journal

Earthquake Engineering and Structural Dynamics, Volume50, Issue9

Published

26 February 2021

URL

<https://doi.org/10.1002/eqe.3437>

この論文は出版社版ではありません。

引用の際には出版社版をご確認のうえご利用ください。

Effects and Dynamic Characteristics of the Core-suspended Isolation System

Assessed by Long-term Structural Health Monitoring

Yutaka Nakamura¹ and Keiichi Okada²

¹ Shimane University, Matsue, Shimane, Japan

² Institute of Technology, Shimizu Corporation, Tokyo, Japan

SUMMARY

The seismic isolation mechanism of the core-suspended isolation (CSI) system comprises a double layer of inclined rubber bearings installed on top of a reinforced core structure. A multi-level structure is then suspended from a hat truss or umbrella girder constructed on the seismic isolation mechanism. The first building to use the CSI system was the Safety and Security Center in Tokyo, Japan, whose structural health monitoring system has detected and recorded 231 earthquake motions since 2006, including the 2011 Tohoku Pacific Earthquake (2011-TPE). The present study estimates the dynamic characteristics of this CSI-equipped building in earthquakes, and the effects of the CSI system are revealed via the observed earthquake records. The temporal changes of the fundamental period and damping factor are estimated from the 2011-TPE; the fundamental period increases with the deformation of the isolation level, whereas the fundamental damping factor is only related weakly to that deformation. The 231 observed earthquake records reveal that the CSI system performs seismic isolation by reducing the response acceleration of the suspended structure by roughly a half for peak ground accelerations exceeding 30 cm/s^2 . Daily microtremor observations are used to diagnose earthquake damage; the fundamental frequencies in each direction remain almost constant and were not changed by the 2011-TPE.

Keywords: core-suspended isolation, inclined rubber bearings, double layer, pendulum, structural health monitoring, seismic observation, 2011 Tohoku-Pacific Earthquake, natural period

Correspondence: Yutaka Nakamura, yutaka.nakamura@riko.shimane-u.ac.jp

1. INTRODUCTION

In areas and countries where the earthquake risk is high, seismic isolation (SI) systems are now used widely to reduce considerably the responses of structures to earthquakes. Various SI methods have been developed and applied to new buildings of all heights, as well as for retrofitting existing buildings without altering their appearance [1-3]. An SI building has an “isolation level” between its foundation and superstructure, and the fundamental principle of any SI system is to have isolators and dampers at the isolation level to decouple the superstructure from the ground and minimize the transmission of earthquake motion. For the superstructure above the isolation level, the fundamental natural period is longer and the acceleration response is much less than the ground acceleration. The isolators are designed to provide low horizontal stiffness, large horizontal deformation capability, and high vertical stiffness to support the superstructure weight in a stable manner; laminated rubber bearings are most often used as the isolators in SI buildings.

The core-suspended isolation (CSI) system has been developed as an utterly new type of SI system [4, 5]. Unlike a conventional SI system, the isolation level of the CSI system is located at the top of the structure. As shown in Figure 1, the CSI system comprises a reinforced concrete core on top of which is installed an SI mechanism comprising a double layer of inclined rubber bearings to create a pendulum isolation mechanism. A multi-level structure is then suspended from a hat truss or umbrella girder constructed on the SI mechanism. The first building to use the CSI system was the Safety and Security Center in Tokyo, Japan.

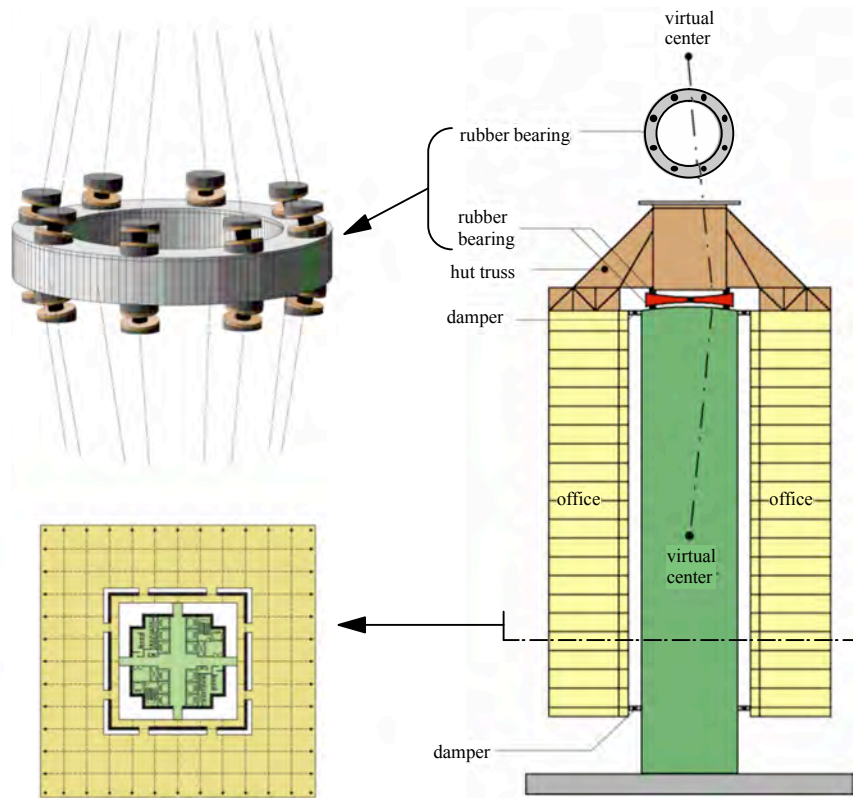
The seismic response of a building can be observed by means of various vibrometers such as seismographs and accelerometers, and the dynamic characteristics of the structure can be evaluated through system identification techniques [6-21]. Structural health monitoring (SHM) is a technology for examining structures physically by using installed sensors and a data acquisition/transmission system [22-24]. SHM can examine the physical condition of a structure under normal conditions and then diagnose any damage or changes due to an earthquake. SHM is quite useful for determining whether an affected structure can be used as it is, or how serious the damage is immediately after an earthquake. In addition, SHM can show how earthquake-proof performance is achieved by monitoring the physical status of the structure directly. The effects of SI systems have been recognized widely through the SHM of SI buildings, and the dynamic characteristics (e.g., fundamental frequency, damping factor) of SI buildings have been evaluated by means of SHM [25-27].

The natural period of a SI building can be evaluated by the eigenvalue analysis of its analytical model in the structural design process where the effects of non-structural elements such as expansion joints are not taken into account. The expansion joints and flexible plumbing between the isolated structure and any adjacent structure own some stiffness and damping properties, and may have considerable influence on the dynamic characteristics and the earthquake responses of the SI building. It is known that the observed natural period of a SI building is shorter than the analytical value and the observed damping factor is bigger than the supposed value, and that the observed dynamic characteristics are not constant and show nonlinearity with respect to the response value. The SHM system is also useful for evaluating the effects of the SI joints and connections that cannot be considered in the stages of structural design and analyses.

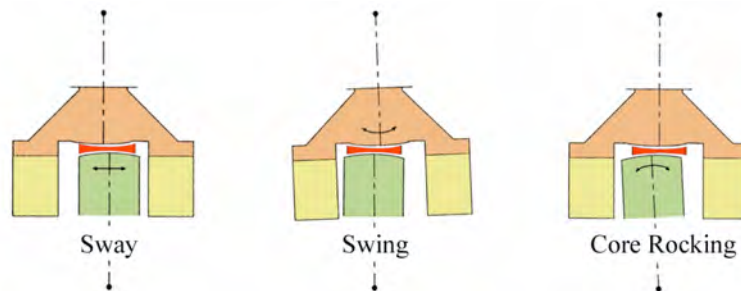
The SHM system of this first CSI building (hereinafter referred to simply as the CSI building) has detected and recorded 231 earthquake motions since 2006, including the 2011 Tohoku Pacific Earthquake (2011-TPE). The SHM system has also been collecting a 2-min microtremor trace at midnight each day. In the present study, the dynamic characteristics of the CSI building in earthquakes are estimated, and the effects of the CSI system are revealed via the observed earthquake records. Earthquake damage is diagnosed based on changes in the normal dynamic characteristics as revealed by the daily microtremor observations.



(a) Conceptual drawing of CSI-equipped buildings



(b). A prototype of a CSI-equipped building



(c). Pendulum isolation mechanism of CSI system

Figure 1. Buildings with core-suspended isolation (CSI) system.

2. STRUCTURAL MECHANICS OF CORE-SUSPENDED ISOLATION

The structural mechanics of the CSI system is reviewed here to illustrate its uniqueness and advantages. The isolation mechanism of the CSI system is located at the top of the core structure, and comprises a double layer of inclined rubber bearings. The upper and lower layers consists of a circular arrangement of rubber bearings that are inwardly inclined with the same tilt angle so as to have a virtual center of rotation above or below the layer, as shown in Figure 1(b).

A simplified model of a structure utilizing the CSI system can be expressed as a 2DOF system as shown in Figure 2. In this figure, m and I_θ are the total mass and the rotational inertia of the suspended structure, respectively; R_1 and R_2 are the lower and upper radii of gyration of the SI mechanism, respectively; K_1 and K_2 are the horizontal stiffnesses of the rubber bearings in the lower and the upper layers, respectively; θ_1 and θ_2 are the rotation angles of the upper and the lower layers, respectively; P is the horizontal force applied at the upper virtual center; u_2 is the horizontal displacement of the center of gravity of the suspended structure.

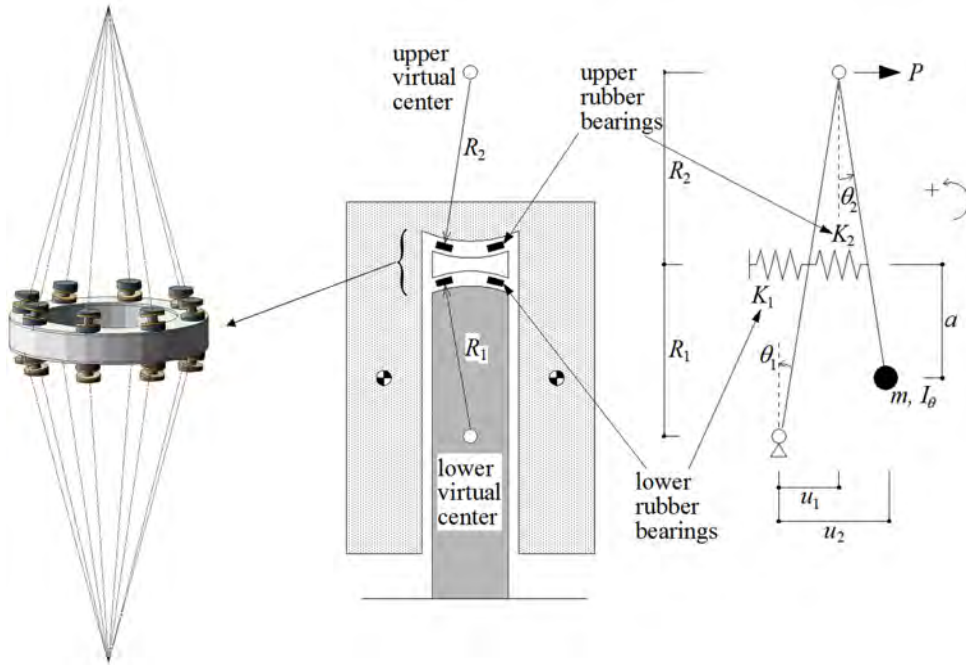


Figure 2. Isolation by a double layer of inclined rubber bearings placed in a circle.

The equations of free vibration with respect to θ_1 and θ_2 are given in the following matrix when defining $\theta_1 = A_1 \exp(i\omega t)$, $\theta_2 = A_2 \exp(i\omega t)$:

$$\begin{bmatrix} -\{I_\theta + m(R_2 + a)^2\} \omega^2 + K_2 R_2^2 + mg(R_2 + a) & m(R_2 + a)(R_1 + R_2) \omega^2 - K_2 R_2^2 \\ m(R_2 + a)(R_1 + R_2) \omega^2 - K_2 R_2^2 & -(R_1 + R_2)^2 \omega^2 + K_1 R_1^2 + K_2 R_2^2 - mg(R_1 + R_2) \end{bmatrix} \begin{Bmatrix} \theta_1 \\ \theta_2 \end{Bmatrix} = \begin{Bmatrix} 0 \\ 0 \end{Bmatrix} \quad (1)$$

The frequency equation can be derived from the condition that the determinant of the above matrix vanishes. The first- and the second-mode periods, T_1 and T_2 , are given by the following equations for the case where $R_1 = R_2 = R$ and $K_1 = K_2 = K$:

$$T_1 = 2\pi \sqrt{\frac{C_1}{C_2 - \sqrt{C_2^2 - C_1 C_3}}}, \quad T_2 = 2\pi \sqrt{\frac{C_1}{C_2 + \sqrt{C_2^2 - C_1 C_3}}} \quad (2)$$

where

$$\begin{aligned} C_1 &= 4mR^2 I_\theta, \quad C_2 = I_\theta (KR^2 - mgR) + mK(R^2 + a^2)R^2 + m^2 g(R^2 - a^2)R \\ C_3 &= 2\{KR^2 + mg(R+a)\}(KR^2 - mgR) - K^2 R^4 \end{aligned} \quad (3a-c)$$

When $R (= R_1 = R_2)$ is infinitely large, the vibration model reduces to a SDOF system with a double-layer of rubber bearings (with horizontal stiffness K) at no inclination. The natural period of this SDOF system is $T_0 = 2\pi\sqrt{2m/K}$. Figure 3 shows the relationship between the radius of gyration, R , and the ratios of the first- and second-mode periods, T_1/T_0 and T_2/T_0 , normalized to the natural period of the associated SDOF system with no bearing inclination, T_0 , for a prototype of a CSI-equipped building in Figure 1(b). Figure 3 demonstrates that the natural periods of the CSI building become longer with decreasing radius of gyration, R . Figure 4 shows the first and second mode shapes for $R=50$ m. It is seen that in the first mode, the lower and the upper layer of bearings deform in the same direction, with the upper layer's deformation being greater than that of the lower. In the second mode, the deformation of the lower bearing is predominant.

The tilting of the rubber bearing (or decreasing the radius of gyration) in the upper and the lower layers of the CSI mechanism can elongate the natural period of the suspended structure several times beyond that of a standard isolation system with no bearing inclination. Nakamura et al. carried out shaking table tests of the CSI system, and demonstrated that tilting of the rubber bearings elongates the natural periods in accordance with the theory [5].

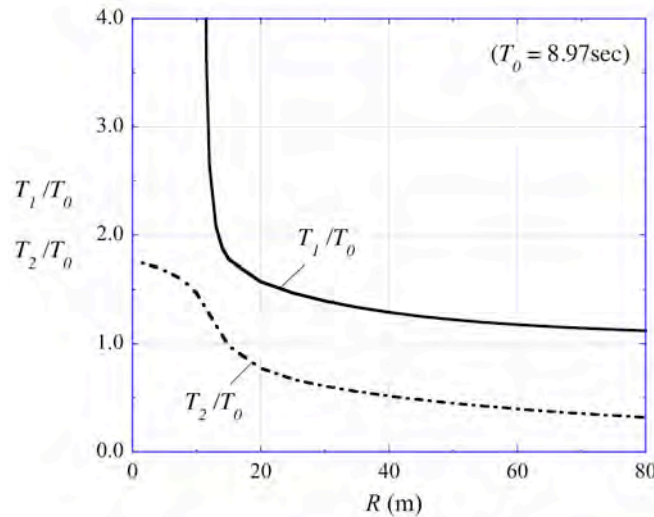


Figure 3. Relationship between the radius of gyration and the normalized first and second mode periods of a CSI-equipped 2DOF model.

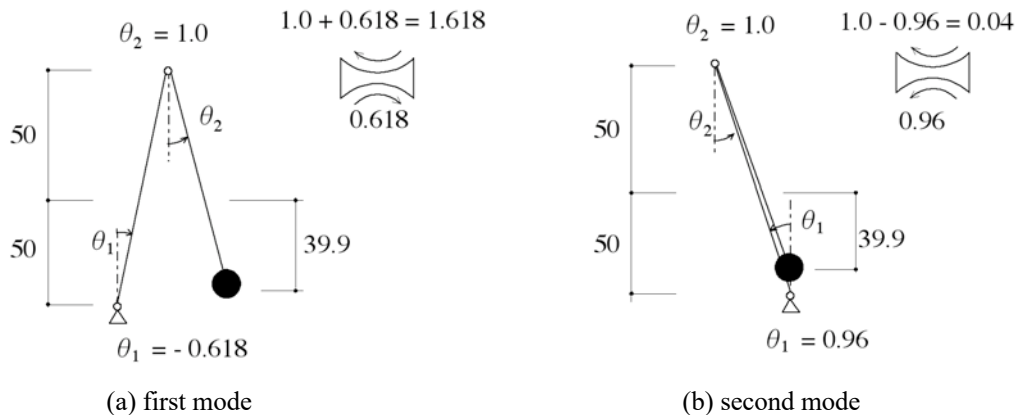


Figure 4. The first and second mode shapes of a CSI 2DOF model for $R=50$ m.

In the CSI system, the tilt angle is able to regulate the earthquake response without adjusting the stiffness of the rubber bearings and to play the role of a design parameter that is not available for conventional rubber bearing-based seismic isolation systems. The CSI system can combine the SI effect and the architectural advantages of a suspended structure. Since steel bars, rods or cables are used for suspension members, the structure can have open and transparent façades. The bottom level can be column-free and provide open space, as illustrated in Figure 1.

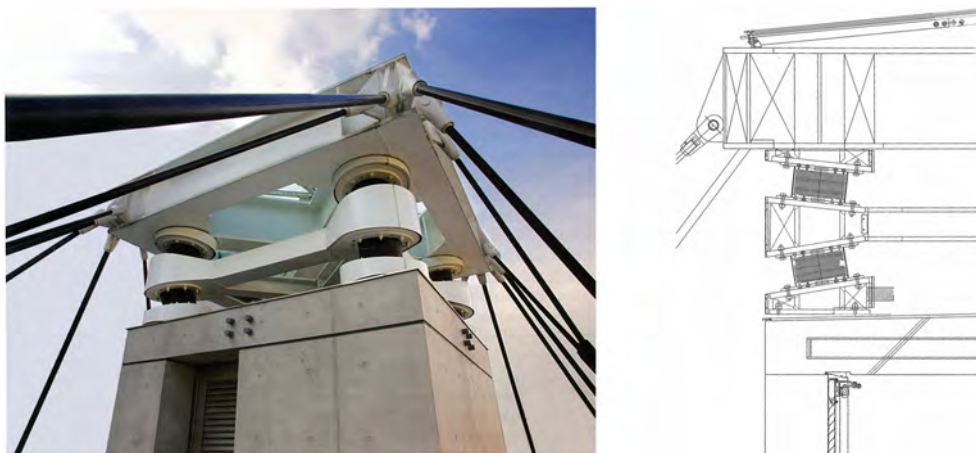
3. BUILDING EQUIPPED WITH CORE-SUSPENDED ISOLATION

The present CSI building is shown in Figure 5 and the design details are given in Table 1. The building's SI mechanism comprises two layers each of four inclined rubber bearings installed at the top of a reinforced concrete core, from which three floors of office structure are suspended by high-strength steel rods [4, 5]. The suspended office structure moves separately from the core structure, and expansion joints are installed between them at all floor levels, as shown in Figure 6.

Fluid dampers as shown in Figure 7 are installed between the core shaft and the suspended office structure at the second floor and rooftop levels (Figure 8). These dampers use a safety locking mechanism that is normally locked to brace the office structure against wind loads but that is released automatically in the event of an earthquake when the ground motion exceeds a threshold value. The latter is set as 5 cm/s^2 and 8 cm/s^2 RMS over 1 s in the horizontal and vertical directions, respectively.



(a) Photograph (left) and perspective drawing (right) of first CSI-equipped building



(b) Pendulum seismic isolation (SI) mechanism comprising two layers each of four inclined rubber bearings

Figure 5. First CSI building: the Safety and Security Center.

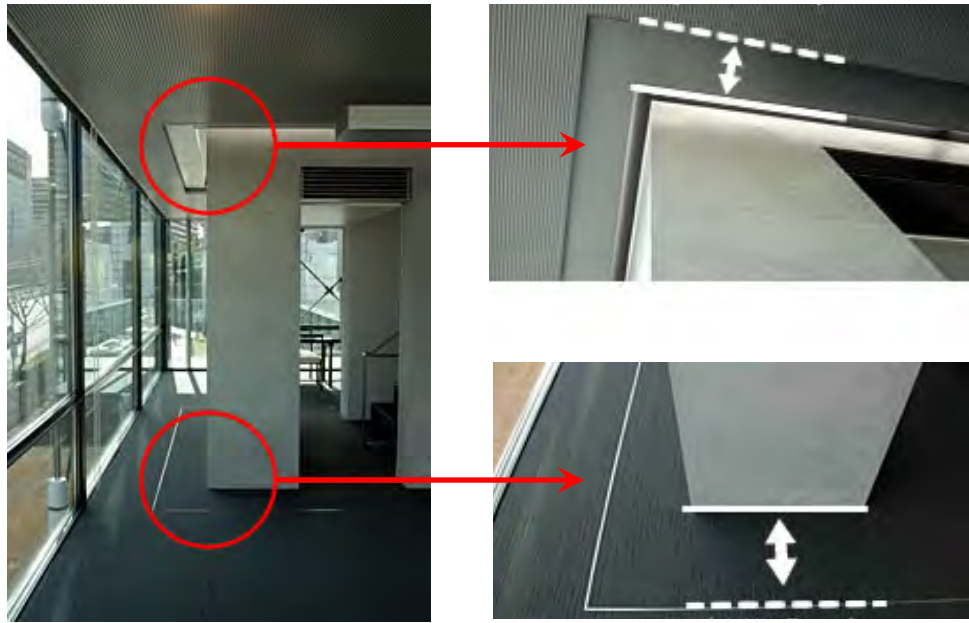
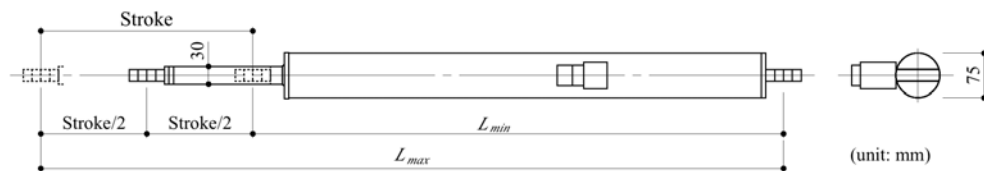


Figure 6. Expansion Joints between concrete core and suspended office structure of CSI building

Table 1. Details of Safety and Security Center.

Floor area	Total: 213.65 m ² ; first floor: 9.05 m ² ; second-to-fourth floors: 66.15 m ² ; penthouse: 6.15 m ²
Height	Total: 18.75 m; first floor: 4.15 m; second-to-fourth floors: 3.0 m
Core shaft	Reinforced concrete wall; 200-mm thick; 400-mm clearance joint
Suspended structure	Total weight: 180 ton; steel rod column 42-mm diameter Two layers each of four inclined rubber bearings
Rubber bearings	Diameter: 300 mm; inner steel shims: 1.2 mm × 45; rubber layers: 2.1 mm × 46; S1 = 35.7; S2 = 3.11; G = 0.29 MPa; horizontal stiffness = 215 kN/m Allowable horizontal deformation: 155 mm
Tilt angles	Lower layer: $\phi_1 = 9.9^\circ$ ($R_1=9.5$ m); upper layer: $\phi_2 = 6.6^\circ$ ($R_2=14.25$ m)
Fluid dampers	Two dampers at second floor and four at rooftop level in X and Y directions
First-mode periods	5.08 s in X direction; 5.14 s in Y direction (analytical values)



Maximum force [kN]	Limiting speed [m/s]	L_{min} [mm]	L_{max} [mm]	Stroke [mm]	Damping coefficient [kN s/m]	Lock force [kN]
50	1.0	1480	2200	720	50	50

Figure 7. Fluid damper with safety locking mechanism.

Eigenvalue analyses of the analytical model without fluid dampers and the expansion joints revealed that the sway motion of the suspended structure was predominant in the first mode and the first mode period was around 5 seconds in both the X and Y directions, as shown in Figure 8.

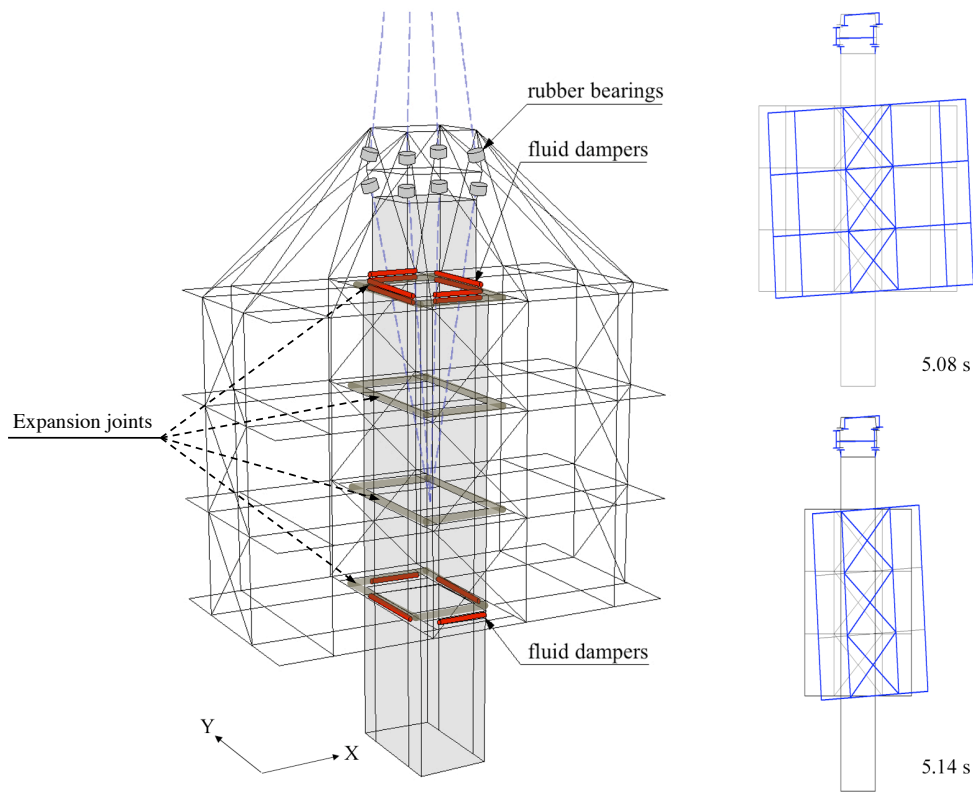


Figure 8. Analytical model and first mode shapes in X and Y directions.

4. STRUCTURAL HEALTH MONITORING IN CSI BUILDING

An SHM system was implemented in the CSI building to detect the seismic performance [23]. Figure 9 shows the sensor arrangements (seven accelerometers, two displacement meters, and one wind anemometer), and a block diagram of the SHM system in the building. This system detects and records seismic vibrations when the observed acceleration of any accelerometer in any direction exceeds 3 cm/s^2 RMS for more than 1 s. When the control system receives the observed data from the sensors, the information display indicates an earthquake occurrence, and the fluid dampers are unlocked if the ground motion exceeds the threshold value.

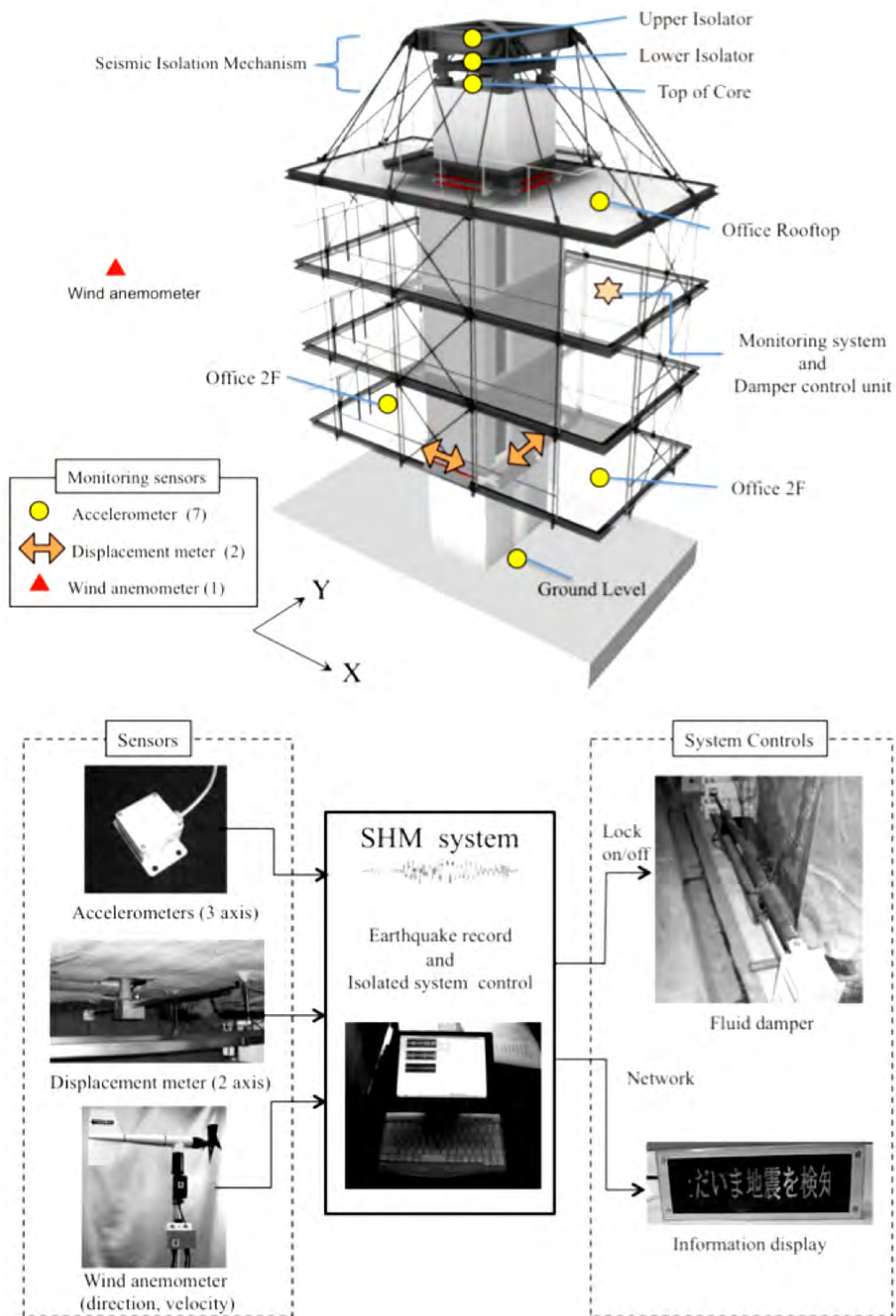


Figure 9. Structural health monitoring (SHM) system installed in CSI building.

4. RESPONSE OF CSI BUILDING TO 2011 TOHOKU PACIFIC EARTHQUAKE

4.1 Effects of 2011 Tohoku Pacific Earthquake on CSI System

The maximum acceleration responses of the Safety and Security Center when subjected to the 2011-TPE are shown in Figure 10 [25]. Although the acceleration responses were amplified at the top of the core structure, the CSI system reduced them: compared to those on the ground, the maximum accelerations on the floors in the hung structure were reduced to about half in the X direction and to about one third in the Y direction. The observed acceleration waves in the Y direction on the ground level and on the second floor in the office are shown in Figure 11.

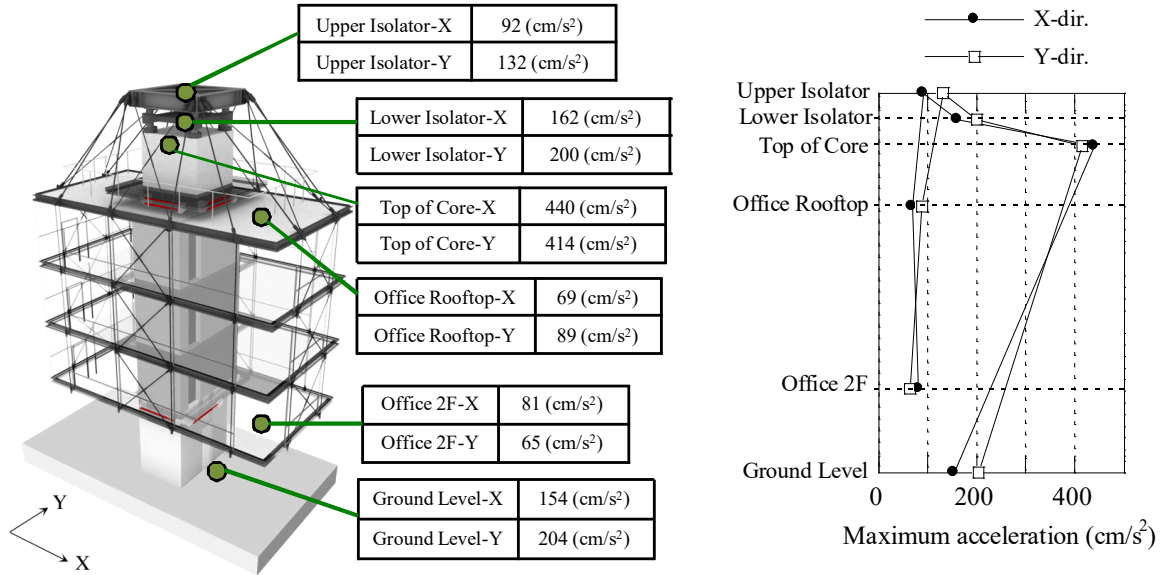


Figure 10. Maximum responses of CSI building.

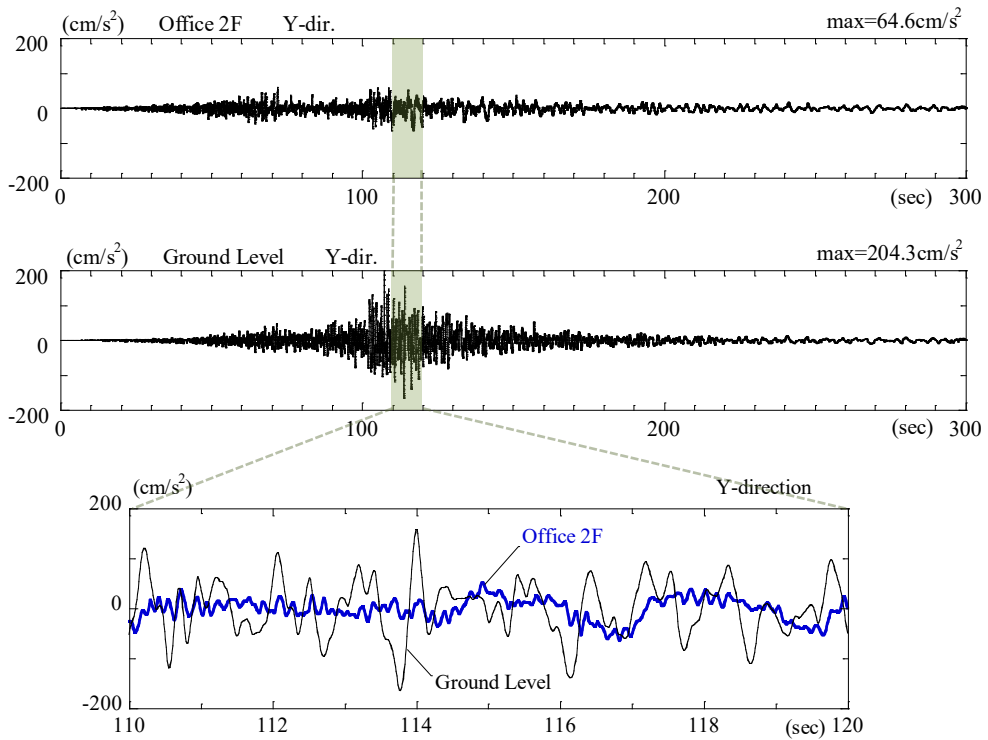


Figure 11. Observed acceleration waves on ground level and in an office on second floor of CSI building.

Figure 12 shows the locus of the horizontal relative displacement of the isolation level, that is, the SI mechanism comprising two layers each of four inclined rubber bearings. The deformation wave of the isolation level in each horizontal direction, D_x or D_y , was obtained from the difference between the double-integrated acceleration wave of the upper isolator and that of the top of core, which is shown later in Figures 16(a) and 17(a). The maximum horizontal relative displacement of the isolation level was 6.86 cm.

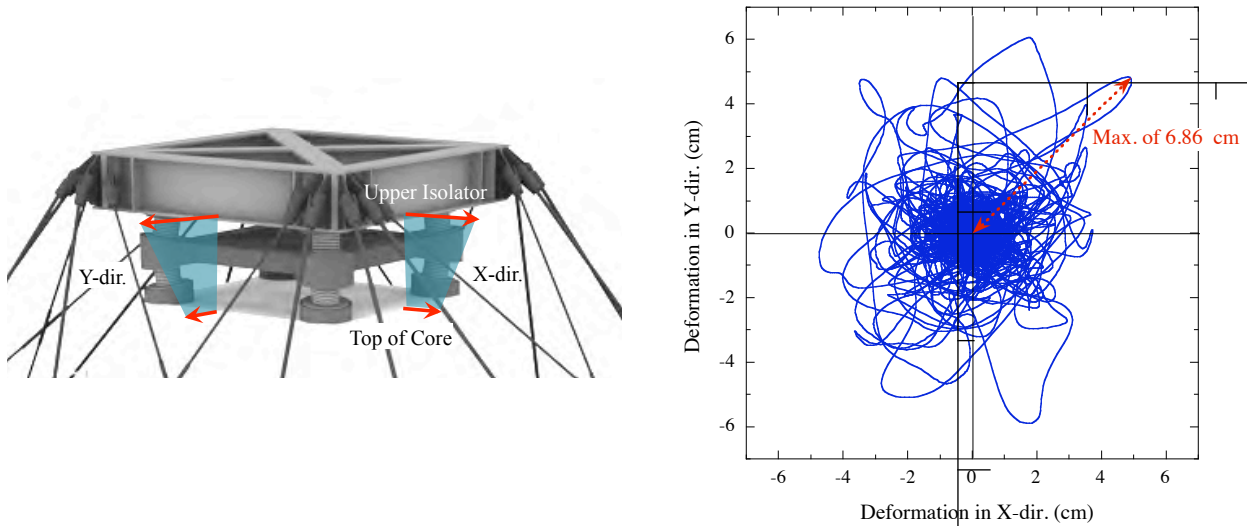


Figure 12. Locus of horizontal relative displacement of SI mechanism.

Figure 13 shows the estimated participation vector of the first mode in the X and Y directions, which were calculated from the vibration model estimated by the system identification method in the following section. The mode shape of the SI mechanism on the core structure dominated. The sway motion of the suspended structure was predominant and the small swing motion of the suspended structure was observed in the first mode in both directions.

Figure 14 shows the transfer functions between the isolated structure and the ground and those between the core structure and the ground in the X and Y directions. Figure 14 indicates the effect of the SI mechanism and the dynamic characteristics of the core structure.

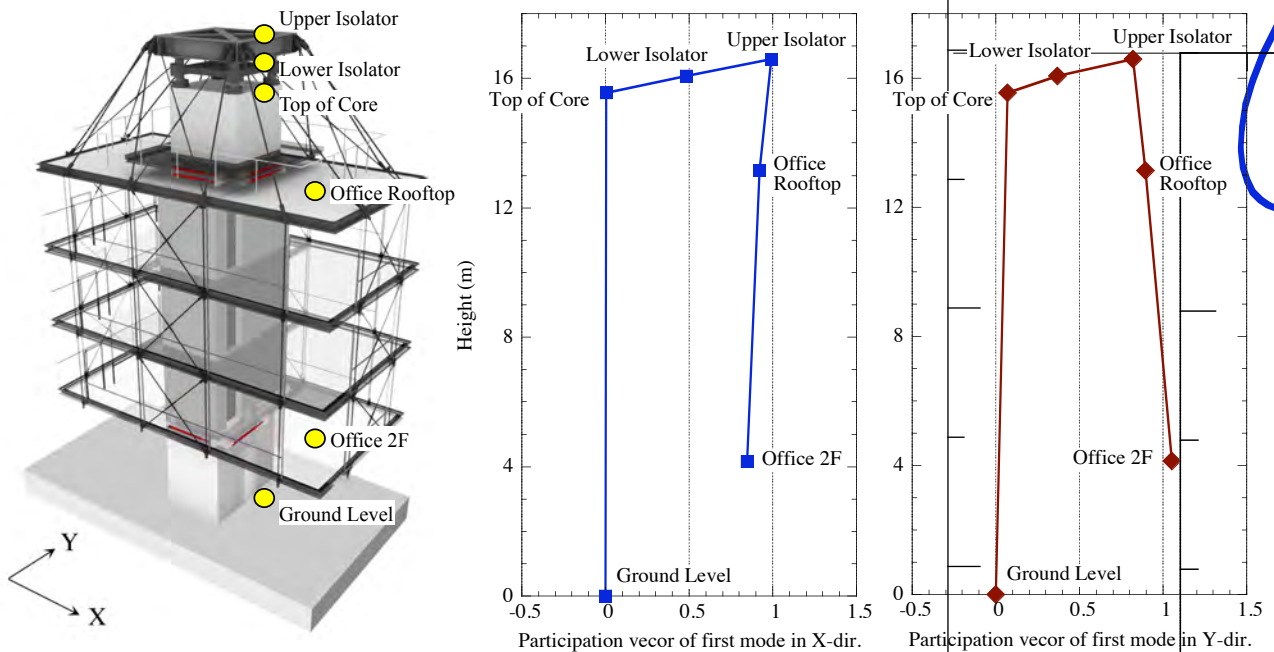
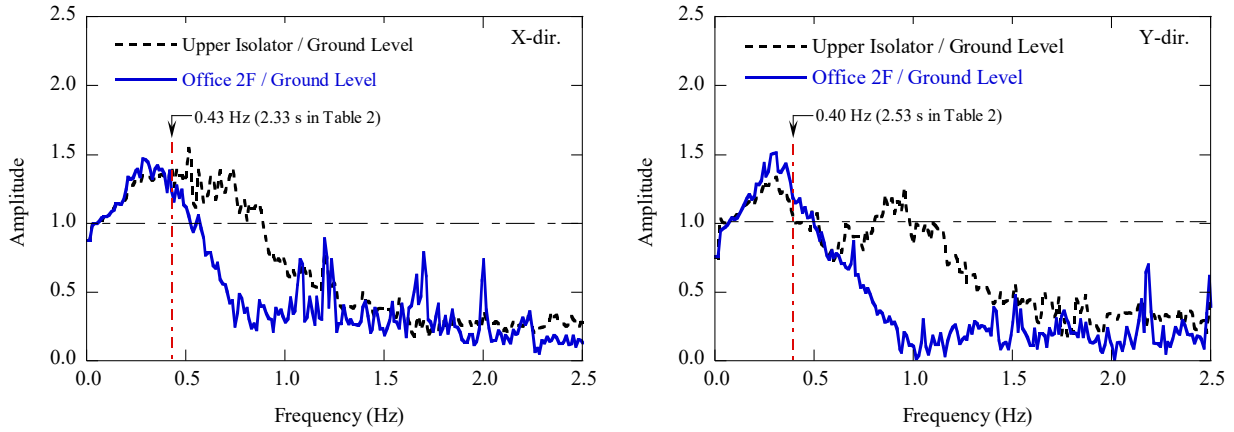
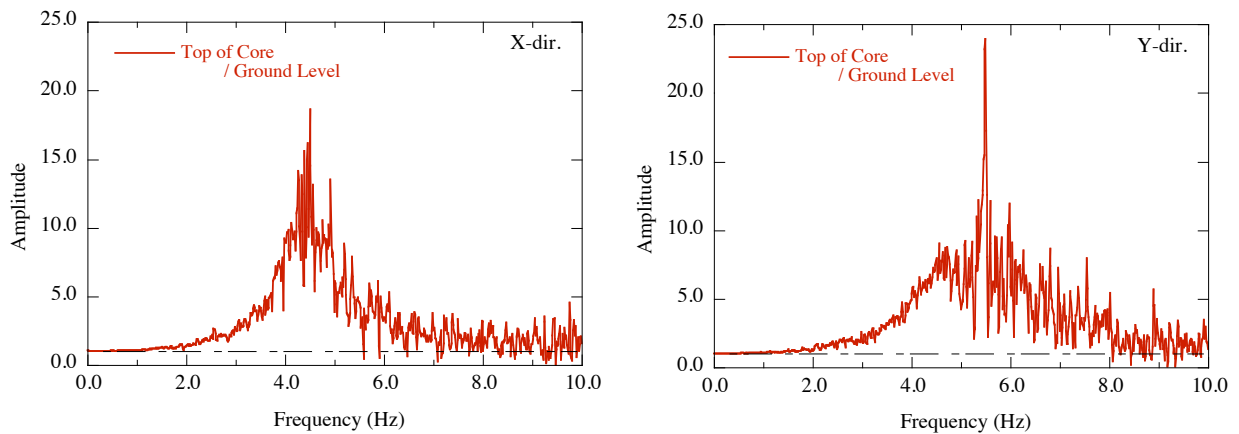


Figure 13. Estimated participation vector of first mode in X and Y directions.

Figure 14(b) shows that the reinforced concrete core fixed on the ground has the resonant frequency in the range of 4-5 Hz in the X-direction and in the range of 5-6 Hz, respectively, and that the peak amplitude of the transfer function reaches 20 in both directions. Figure 14(a) shows that the resonant frequency of the SI mechanism is lower than 0.5Hz in both directions, which corresponds roughly with the estimated value in Table 2 in the following section, and that the peak amplitude of the transfer function remains at 1.5 in both directions. Figure 15 shows the power spectrum densities (PSD) at the top of the core and an office on the second floor in X and Y directions. The strength of PSD in the suspended office is much weaker than that at the top of the core.



(a) Amplitudes of transfer functions between isolated structure and ground in X and Y directions



(b) Amplitudes of transfer functions between core structures and ground in X and Y directions

Figure 14. Transfer functions of isolate structure and core structure in X and Y directions.

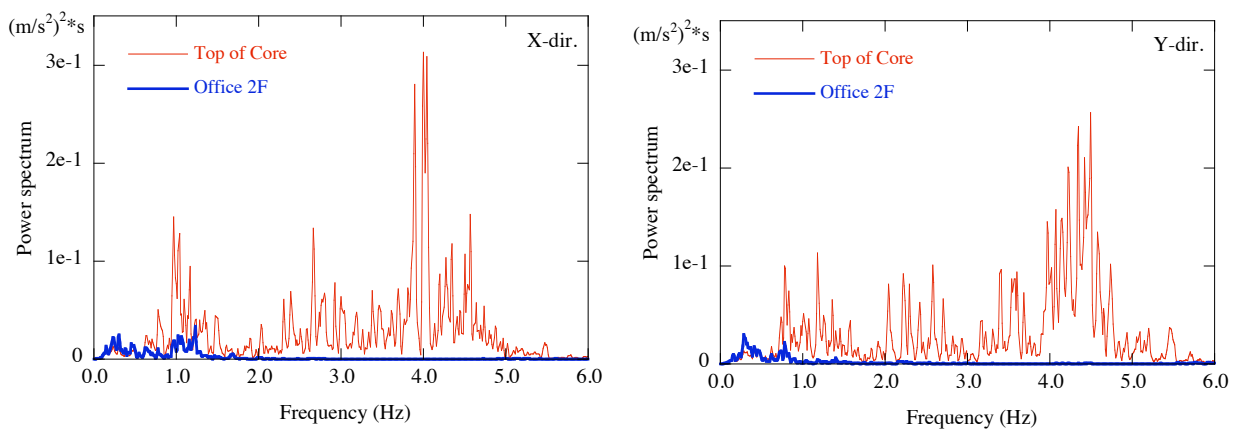


Figure 15. Power spectrum densities at top of core and an office on second floor in X and Y directions.

4.2 Dynamic Characteristics of CSI System from 2011 Tohoku Pacific Earthquake

The dynamic characteristics of the building, namely the fundamental natural period and damping, were estimated from the 2011-TPE. An auto-regressive exogenous input (ARX) model [10, 14, 15, 19, 20] as shown in Figure 16 and Equations (4)-(7) was applied to the observed acceleration waves by assigning the wave on the ground level as the input and the two waves on the office rooftop and on the office second floor as two outputs in each horizontal direction.

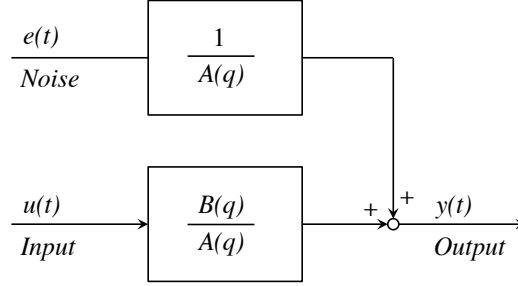


Figure 16. Auto-regressive exogenous input (ARX) model (time domain).

$$A(q)y(t) = B(q)u(t) + e(t) \quad (4)$$

$$\text{where } A(q) = 1 + \sum_{j=1}^{n_a} a_j q^{-j}, \quad B(q) = [B_{mn}(q)], \quad B_{mn}(q) = \sum_{j=1}^{m n b} b_j q^{-j+1-n_k} \quad (5a-c)$$

where a_j and b_j indicate the parameters of the system, and n_a and n_b indicate the orders of $A(q)$ and $B(q)$, respectively, and q^{-j} indicates the backward-shift operator, where q^{-j} is defined as $q^{-j}y(t) = y(t-j)$. The polynomial ratio $B(q)/A(q)$ can be regarded as the system transfer operator. The natural circular frequency ω_k and damping factor h_k can be obtained from the k -th complex root p_k of the polynomial $A(q) = 0$ by the following equations [8, 19]:

$$\omega_k = \ln[1/|p_k|]/(h_k \cdot \Delta), \quad h_k = \ln(1/|p_k|) / \sqrt{\{\tan^{-1}(p_k^I/p_k^R)\}^2 + \{\ln(1/|p_k|)\}^2} \quad (6a, b)$$

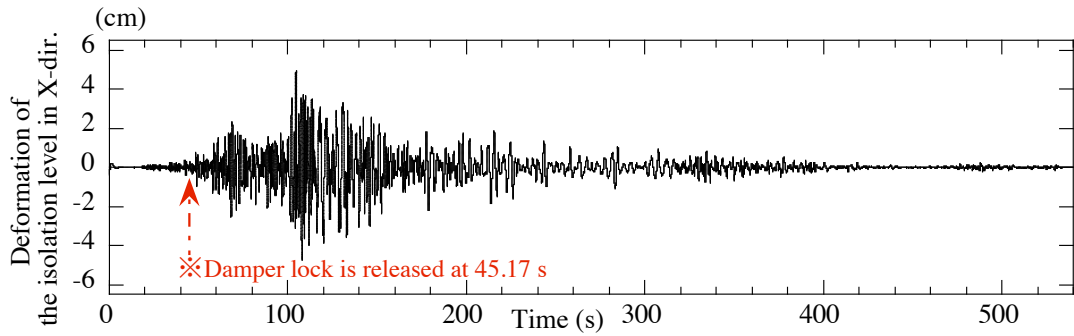
where p_k^R and p_k^I indicate the real and imaginary part of p_k , respectively, Δ indicates the sampling period, and $q^{-1} = e^{-j\omega\Delta}$. The ARX model was able to evaluate the temporal variation of the dynamic characteristics of the building over the observed acceleration waves, which is unachievable by the conventional frequency analysis shown in Figures 14 and 15.

Figures 17 and 18 show how the dynamic characteristics of the building vary in the X and Y directions, respectively. The locking mechanism of the fluid damper (Figure 7) was released automatically at the time of 45.17 s. Figure 17(b) and (c) show the temporal changes of the estimated fundamental period T_{1x} and damping factor h_{1x} , respectively, in the X direction for every 10-s duration. Figure 17(d) and (e) show the relationship between D_x and T_{1x} and that between D_x and h_{1x} , respectively. In the same way, Figure 18(b) and (c) show the temporal changes of the estimated fundamental period T_{1y} and damping factor h_{1y} , respectively, in the Y direction for every 10-s duration, and Figure 18(d) and (e) show the relationship between D_y and T_{1y} and that between D_y and h_{1y} , respectively.

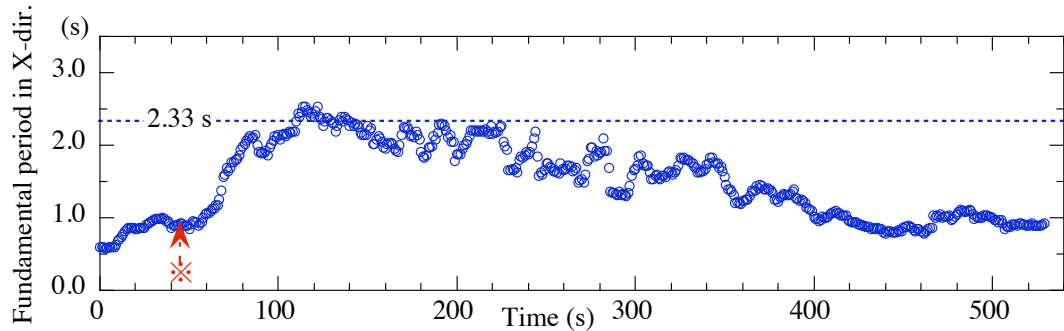
The average values of \bar{T}_{1x} , \bar{T}_{1y} , \bar{h}_{1x} , and \bar{h}_{1y} evaluated from the total observed records are presented in Table 2 and Figures 17(b) and (c) and 18(b) and (c). Figures 17(d) and 18(d) indicate that T_{1x} and T_{1y} increase with D_x and D_y , respectively, while h_{1x} and h_{1y} vary widely and are related only weakly to D_x and D_y as indicated in Figures 17(e) and 18(e). The average fundamental period \bar{T}_{1x} and \bar{T}_{1y} , are not the kind of arithmetic mean of T_{1x} and T_{1y} , and are regulated by the large amplitude of D_x and D_y , respectively.

Table 2. Average fundamental periods and damping factor evaluated from total observed records.

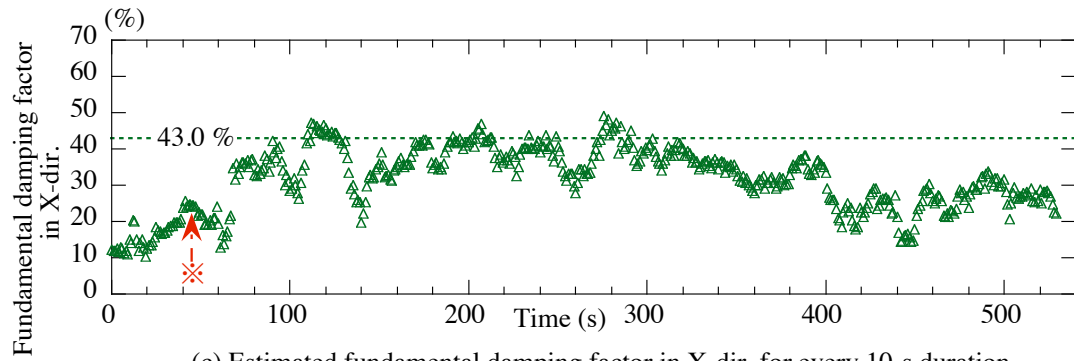
	X direction	Y direction
Fundamental period	$\bar{T}_{1x} = 2.33$ s	$\bar{h}_{1x} = 43.0$ %
Fundamental damping factor	$\bar{T}_{1y} = 2.53$ s	$\bar{h}_{1y} = 47.6$ %



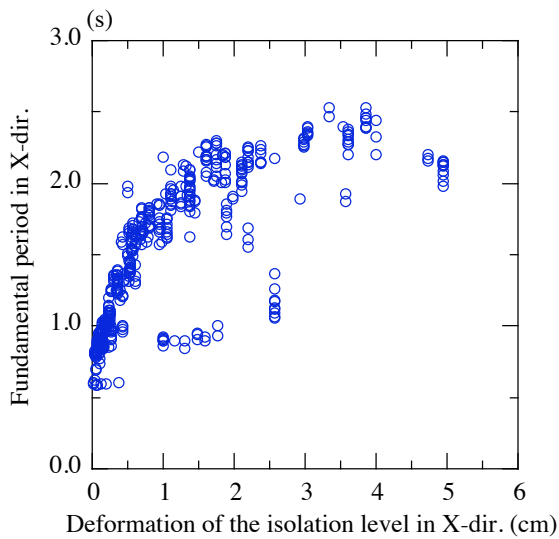
(a) Calculated deformation waves of the isolation level in X-dir.



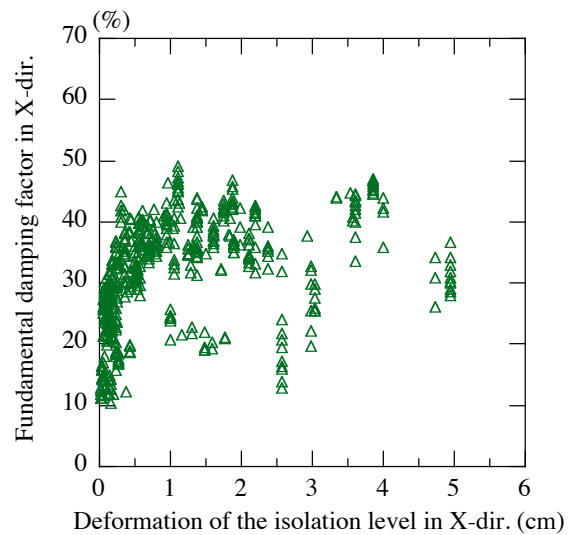
(b) Estimated fundamental period in X-dir. for every 10-s duration



(c) Estimated fundamental damping factor in X-dir. for every 10-s duration

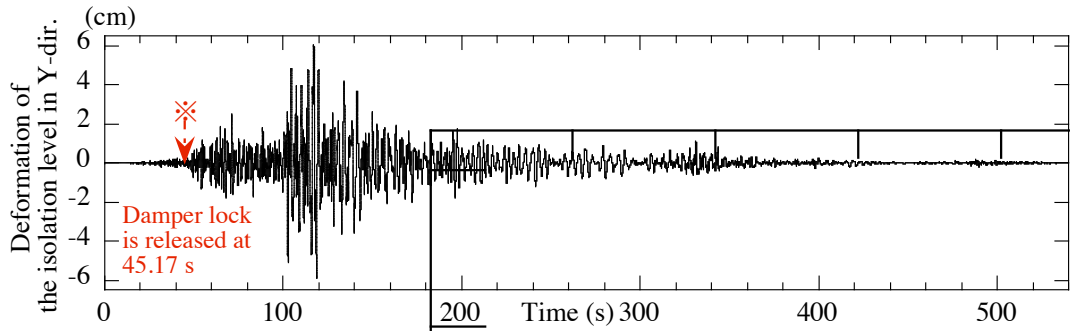


(d) Relationship between deformation of the isolation level and fundamental period in X-dir.

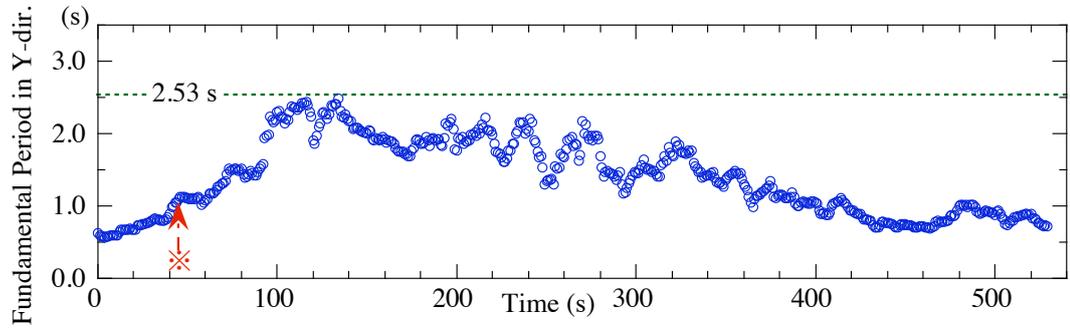


(e) Relationship between deformation of the isolation level and fundamental damping factor in X-dir.

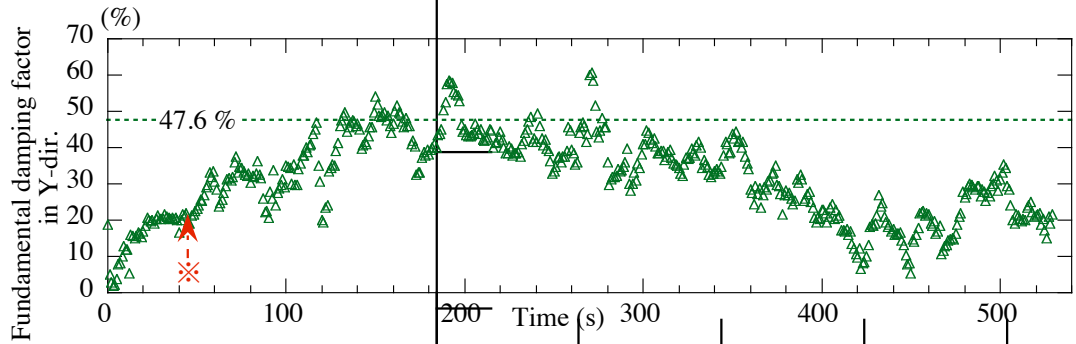
Figure 17. Variations of dynamic characteristics of CSI building in X direction.



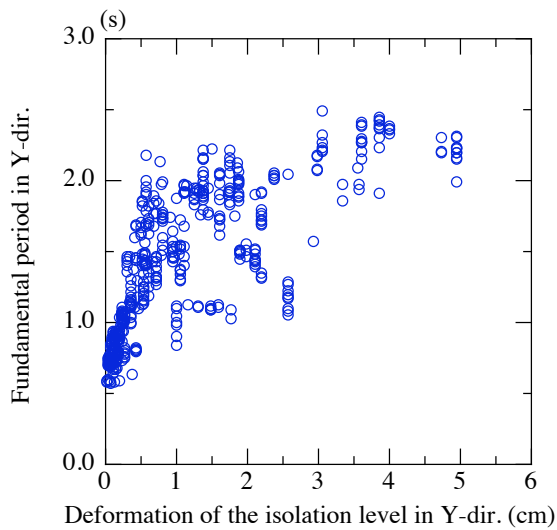
(a) Calculated deformation waves of the isolation level in Y-dir.



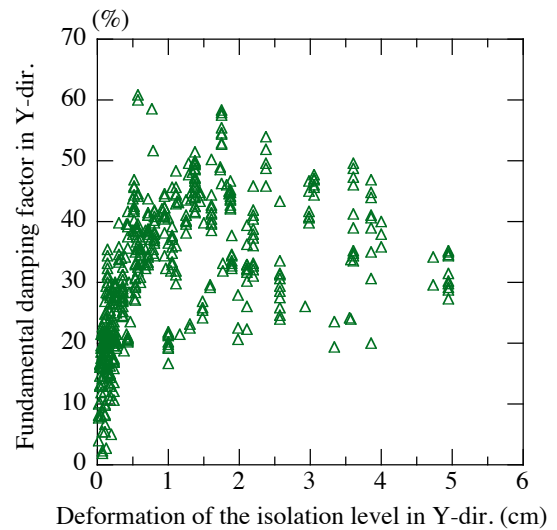
(b) Estimated fundamental period in Y-dir. for every 10-s duration



(c) Estimated fundamental damping factor in Y-dir. for every 10-s duration



(d) Relationship between deformation of the isolation level and fundamental period in Y-dir.



(e) Relationship between deformation of the isolation level and fundamental damping factor in Y-dir.

Figure 18. Variations of dynamic characteristics of CSI building in Y direction.

5. EFFECTS OF CSI SYSTEM FROM LONG-TERM SHM

5.1 Effects of CSI system from 231 Earthquakes

The SHM system of the Safety and Security Center (Figure 9) records seismic vibrations when the observed acceleration of any accelerometer in any direction exceeds 3 cm/s² RMS for more than 1 s. Furthermore, the control system unlocks the fluid dampers when the observed ground motion exceeds 5 cm/s² RMS for more than 1 s in the horizontal direction, or 8 cm/s² RMS for more than 1 s in the vertical direction. The SHM system has recorded 231 earthquake motions since 2006, including the 2011-TPE.

Figure 19 shows the amplification characteristics of the core structure relative to the ground level. The observed peak acceleration $a_{max}^{Top-core}$ on the top of the core structure is amplified up to six times as compared with a_{max}^{Ground} on the ground level. The amplification factor $a_{max}^{Top-core}/a_{max}^{Ground}$ varies widely and has almost no relation to a_{max}^{Ground} or the locked/released condition of the fluid dampers.

Figure 20 shows the transfer characteristics of the CSI mechanism that consists of two layers each of four inclined rubber bearings. The transfer rate is obtained as the ratio of the observed peak acceleration $a_{max}^{Upper-isolator}$ on the upper isolator to $a_{max}^{Top-core}$ on the top of the core structure. The transfer rate $a_{max}^{Upper-isolator}/a_{max}^{Top-core}$ clearly decreases with $a_{max}^{Top-core}$ and falls below unity for $a_{max}^{Top-core} > 10$ cm/s² and below a half for $a_{max}^{Top-core} > 30$ cm/s². Note that the transfer characteristics is unaffected by the locked/released condition of the fluid dampers.

Figure 21 shows the SI effects on the second floor in the CSI building relative to the ground level. The other amplification factor is obtained as the ratio of the observed peak acceleration $a_{max}^{2nd-floor}$ on the second floor to a_{max}^{Ground} on the ground level. The amplification factor $a_{max}^{2nd-floor}/a_{max}^{Ground}$ decreases with a_{max}^{Ground} and falls below unity for $a_{max}^{Ground} > 10$ cm/s², which is when the locks of the fluid dampers are released. Figure 21 shows that the CSI system brings about the SI effect of reducing the response acceleration of the suspended structure by roughly half for $a_{max}^{Ground} > 30$ cm/s².

5.2 Dynamic Characteristics from Daily Microtremor Measurements

The SHM system has also been collecting a 2-min microtremor trace at midnight each day since December 2006. Figure 22 shows the estimated fundamental period in the horizontal X and Y directions for 3898 days when the fluid dampers were locked. The fundamental period in each direction was much shorter than the observed value during the earthquake response, and remained almost constant over the observation period, exhibiting no distinct change after the 2011-TPE. These results imply that the building suffered no structural damage from the 231 observed earthquake events including the 2011-TPE.

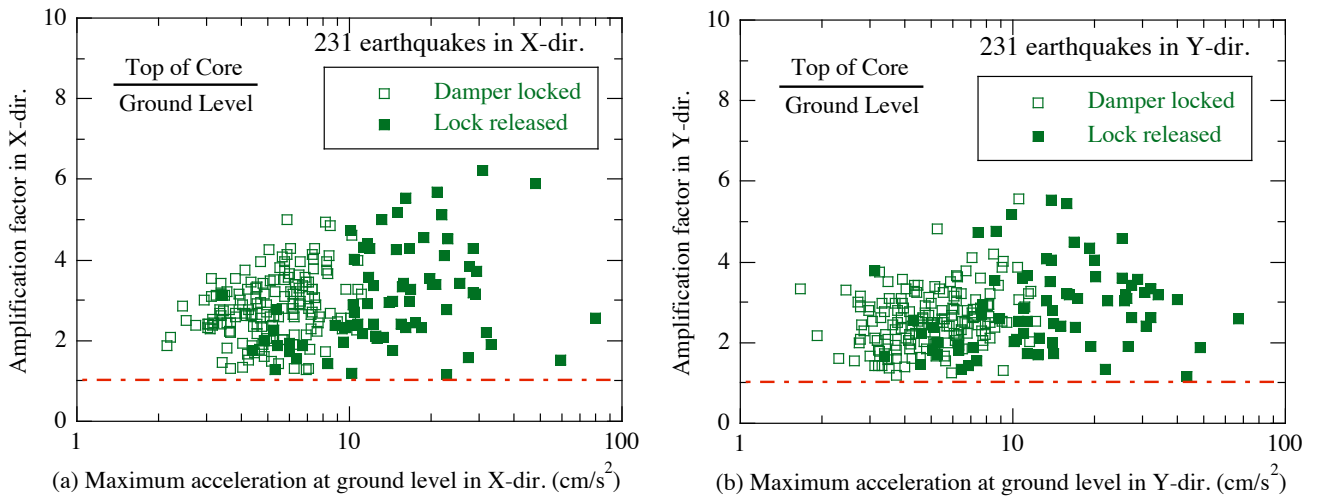


Figure 19. Amplification characteristics of core structure relative to ground level.

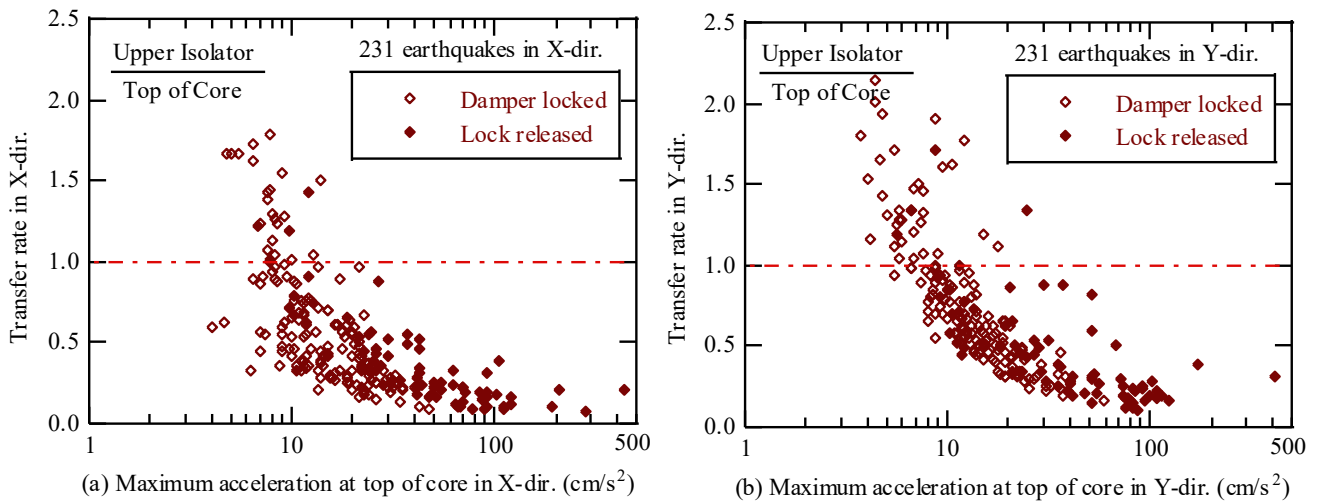


Figure 20. Transfer characteristics of CSI mechanism comprising two layers each of four inclined rubber bearings.

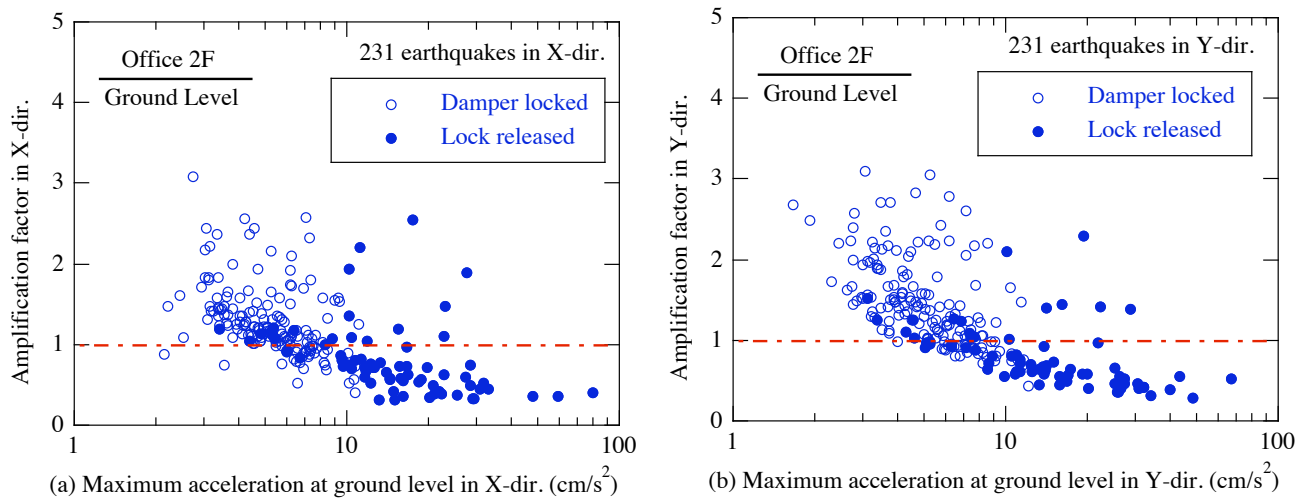


Figure 21. SI effects on second floor of CSI building relative to ground level.

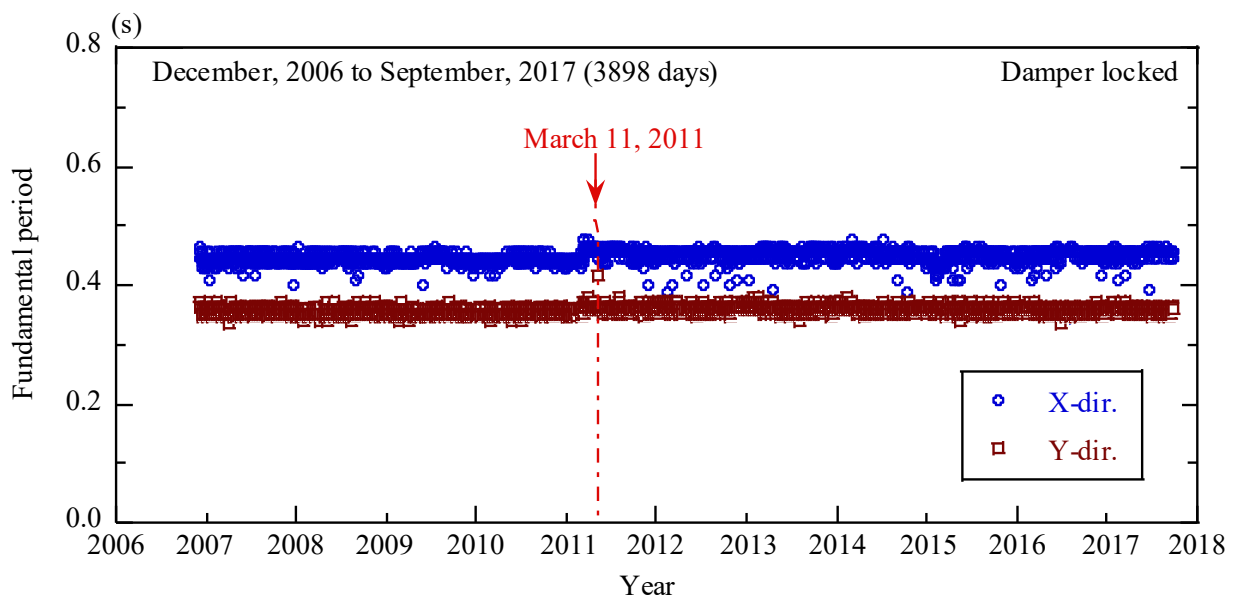


Figure 22. Variations of fundamental period estimated from daily microtremor measurements.

6. CONCLUSION

The CSI system has been developed as an utterly new type of SI system. The CSI system comprises a reinforced concrete core on top of which is installed an SI mechanism comprising a double layer of inclined rubber bearings to create a pendulum isolation mechanism. The tilt angle of the rubber bearings is able to regulate the earthquake response without adjusting the stiffness of the rubber bearings and to play the role of a design parameter that is not available for conventional SI systems. The CSI system can combine the SI effect and the architectural advantages of a suspended structure. Since steel bars, rods or cables are used for suspension members, the structure can have open and transparent façades. The bottom level can be column-free and provide open space.

The Safety and Security Center in Tokyo, Japan was the first building to use the CSI system. The SI mechanism for the building comprises two layers each of four inclined rubber bearings installed at the top of a reinforced concrete core, from which three floors of office structure are suspended by high-strength steel rods. The suspended office structure moves separately from the core structure, and expansion joints are installed between them at all floor levels. Fluid dampers with a safety locking mechanism are installed between the core shaft and the suspended office structure at the second floor and rooftop levels. An SHM system was installed in the Safety and Security Center and has detected and recorded 231 earthquake motions since 2006, including the 2011-TPE, and has been collecting a 2-min microtremor trace each day.

In a SI building, the expansion joints and flexible plumbing between the isolated structure and any adjacent structure own some stiffness and damping properties, and have considerable influence on the dynamic characteristics and the earthquake responses of the SI building. It is known that the observed natural period of a SI building is shorter than the analytical value and the observed damping factor is bigger than the supposed value, and that the observed dynamic characteristics are not constant and show nonlinearity with respect to the response value. The SHM system installed in the Safety and Security Center evaluates the effects of the SI joints and connections that cannot be considered in the stages of structural design and analyses, and the nonlinearity of the dynamic characteristics and the SI effects.

The 2011-TPE revealed the effect of the CSI system of the building. Compared with the maximum acceleration on the ground, the CSI system reduced those on the floors in the suspended structure to roughly a half in the X direction and a third in the Y direction. The temporal changes of the fundamental period and damping factor during the 2011-TPE were estimated based on an ARX model by assigning the wave on the ground level as the input and the two waves on the office rooftop and on the office second floor as two outputs in each horizontal direction. In each direction, the fundamental period of the CSI building is found to be much shorter than the analytical value, and the fundamental damping factor is found to be bigger than the supposed value. The fundamental period increases with the deformation of the isolation level, while the fundamental damping factor is related only weakly to that deformation.

The 231 observed earthquake records reveal the SI features of the CSI system. The CSI two-layered isolator can reduce the peak acceleration on the upper isolator by half compared to the one on the top of the core structure for over 30 cm/s^2 , irrespective of the locked/released condition of the fluid dampers. The CSI system realizes the SI effect of reducing the response acceleration of the suspended structure to roughly half for the peak ground acceleration over 30 cm/s^2 .

The 3898 days of daily microtremor measurements enable any building damage due to earthquakes to be diagnosed. The fundamental periods in the horizontal X and Y directions remain almost constant over the observation period and show no distinct change after the 2011-TPE. These results imply that the building suffered no structural damage from the 231 observed earthquake events including the 2011-TPE.

The CSI system has been developed as an utterly new type of SI system. The SHM system installed in the Safety and Security Center has revealed the dynamic properties of the building and shown the effectiveness of the CSI system at reducing the response acceleration of the suspended structure. These results can help future developments and applications of the CSI system.

ACKNOWLEDGMENTS

The present CSI system was studied in joint research between Tokyo Institute of Technology, Ove Arup & Partners (Tokyo), Daiichi-Kobo Associates, and Shimizu Corporation. The authors would like to thank Prof. Akira Wada, Prof. Toru Takeuchi, Mr. Shigeru Hikone, and Mr. Teiichi Takahashi for their collaboration in developing the CSI system.

DATA AVAILABILITY STATEMENT

Due to the nature of this research, participants of this study did not agree for their data to be shared publicly, so supporting data is not available.

REFERENCES

1. Naeim F, Kelly J. *Design of Seismic Isolated Structures: from theory to practice*. John Wiley & Sons, Inc., New York, 1999.
2. Higasino M, Okamoto S. *Response Control and Seismic Isolation of Buildings*. Taylor & Francis, New York, 2006.
3. Saito Taiki [chair editor]. *How to Plan and Implement Seismic Isolation for Buildings*. Ohmsha, Tokyo, 2013.
4. Nakamura Y, Saruta M, Nakanishi T, Wada A, Takeuchi T, Hikone S, Takahashi T. Development of the core-suspended isolation system. *Proceedings of the 14th World Conference on Earthquake Engineering*, Beijing, China, 2008.
5. Nakamura Y, Saruta M, Wada A, Takeuchi T, Hikone S, Takahashi T. Development of the core-suspended isolation system. *Earthquake Engineering & Structural Dynamics* 2011; 40(4): 429-447. doi:10.1002/eqe.1036.
6. Anderson P. Adaptive forgetting in recursive identification through multiple models. *International Journal of Control* 1985; 42(5):1175-1193.
7. Ljung L. *System Identification*. Prentice Hall, 1987.
8. Şafak E. Adaptive modeling, identification, and control of dynamic structural systems. I: Theory & II: Applications. *Journal of Engineering Mechanics* 1989;115: 2386-2405 & 2406-2426.
9. Çelebi M, Şafak E. Seismic response of Transamerica Building. I: Data and Analysis & II: System Identification. *Journal of Structural Engineering* 1991;117(8):2389-2425.
10. Şafak E. Identification of linear structures using discrete-time filters. *Journal of Structural Engineering* 1991;117(10): 3064-3085.
11. Çelebi M, Şafak E. Seismic response of Pacific Park Plaza. I: Data and Preliminary Analysis & II: System Identification. *Journal of Structural Engineering* 1992;118(6): 1547-1589.
12. Çelebi M. Dynamic characteristics of five tall buildings during strong and low-amplitude motions. *The Structural Design of Tall Buildings* 1993;2:1-15.
13. Şafak E. Response of a 42-storey steel-frame building to the $M_s=7.1$ Loma Prieta earthquake. *Engineering Structures*;1993;15(6):403-421.
14. Saito Tomoo, Okada K, Yokota H. System identification of steel frame buildings through observed earthquake records. Part I and II. *Summaries of technical papers of Annual Meeting, Architectural Institute of Japan*, 1994:673-676. (in Japanese)
15. Okada K, Yokota H. Dynamic characteristics of steel frame buildings using system identification technique, *Proceedings of the 9th Japan Earthquake Engineering Symposium* 1994:1717-1722, Tokyo, Japan. (in Japanese)
16. Loh C, Tou I. A system identification approach to the detection of changes in both linear and non-linear structural parameters. *Earthquake Engineering & Structural Dynamics* 1995;24(1):85-97.
17. Loh, C, Lin H. Application of off-line and on-line identification techniques to building seismic response data. *Earthquake Engineering & Structural Dynamics* 1996;25(3):269-290.
18. Saito Tomoo, Yokota H. Evaluation of dynamic characteristics of high-rise buildings using system identification techniques. *Journal of Wind Engineering & Industrial Aerodynamics* 1996;59(2-3)21:299-307.
19. Saito, Tomoo. System identification of a high-rise building applying multi-input-output ARX model of modal analysis. *Journal of Structural and Construction Engineering, Architectural Institute of Japan* 1998;508:47-54. (in Japanese)

20. Ikeda Y, Hisada Y. Earthquake responses on all floors in a building estimated by observation records on some restricted floors. *Journal of Japan Earthquake Engineering* 2013;13(4):38-54. (in Japanese)
21. Siringoringo DM, Fujino Y. Long-term seismic monitoring of base-isolated building with emphasis on serviceability assessment, *Earthquake Engineering & Structural Dynamics* 2015;44(4):637-655. doi:10.1002/eqe.2538.
22. Okada K, Shiraishi M, Iwaki H, Shiba K. Internet-based remote controlled structure monitoring system. *Structural Health Monitoring and Intelligent Infrastructure. Proceedings of the First International Conference SHMII-01*, Tokyo, Japan, 2003.
23. Okada K, Nakamura Y, Saruta M. Application of earthquake early warning system to seismic-isolated buildings. *Journal of Disaster Research* 2009;4:570-578. doi:10.20965/jdr.2009.p0242.
24. Okada K, Kataoka S. Overall building response estimation method on records from two seismographs. *The Journal of Japan Association for Earthquake Engineering* 2016;16:94-113.
25. Nakamura Y, Hanzawa T, Hasebe M, Okada K, Kaneko M, Saruta M. Report on the seismic isolation methods from the 2011 Tohoku-Pacific Earthquake. *Seismic Isolation and Protection Systems* 2011;2:57-74.
26. Tomizawa T, Takahashi O, Suhara J, Okada K, Tsuyuki Y, Fujita T. A study on earthquake observation record in the building using the three-dimensional seismic isolation system. *Journal of Structural and Construction Engineering, Architectural Institute of Japan* 2012;679:1393-1402. (in Japanese)
27. Yoshimoto R, Mita A, Okada K. Damage detection of base-isolated buildings using multi-input multi-output subspace identification. *Earthquake Engineering & Structural Dynamics* 2005;34:307-324. doi:10.1002/eqe.435.